JGR Oceans

RESEARCH ARTICLE
10.1029/2025JC023611

Persistent Ocean-Shelf Transport Across the North West European Shelf Edge

André Palóczy[1], **Joanne Hopkins**[1], **Anthony Wise**[1], **and John Huthnance**[1]

[1]National Oceanography Centre, Liverpool, UK

Key Points:

- Persistent cross-isobath geostrophic flow is found along the North West European Shelf edge at seasonal and decadal time scales
- The geostrophic flow persists despite strong variability in stratification, due to large-scale, steric, along-isobath sea surface slopes
- The geostrophic cross-isobath flow produces time-mean, depth-integrated nitrate transports of O(1–10 mmol/m/s)

Supporting Information:

Supporting Information may be found in the online version of this article.

Correspondence to:

A. Palóczy,
apaloczy@noc.ac.uk

Citation:

Palóczy, A., Hopkins, J., Wise, A., & Huthnance, J. (2026). Persistent ocean-shelf transport across the North West European shelf edge. *Journal of Geophysical Research: Oceans*, *131*, e2025JC023611. https://doi.org/10.1029/2025JC023611

Received 21 OCT 2025
Accepted 21 JAN 2026

Author Contributions:

Conceptualization: André Palóczy
Data curation: André Palóczy
Formal analysis: André Palóczy
Funding acquisition: Joanne Hopkins
Investigation: André Palóczy, Joanne Hopkins, Anthony Wise
Methodology: André Palóczy
Project administration: André Palóczy
Software: André Palóczy
Validation: André Palóczy
Visualization: André Palóczy
Writing – original draft: André Palóczy
Writing – review & editing: Joanne Hopkins, Anthony Wise, John Huthnance

Abstract Transport mechanisms between the deep ocean and adjacent continental shelf seas play an important role in the spatial distribution of nutrient delivery to the coastal ocean and in the temporal variability of shelf biogeochemical processes. Along the North West European Shelf (NWES) edge, nutrient-rich waters of oceanic origin are found below the mixed layer, representing a potential nutrient source for fueling new production on the shelf. We find persistent cross-isobath geostrophic transport integrated over along-isobath segments of the NWES edge in hydrographic climatologies and altimetric sea surface height gradients. This transport is O(1 cm/s), has little vertical structure, and is onshore along the entire extent of the 200 m isobath, except along the southern rim of the Norwegian Trench. Despite strong temporal variability in the shelf-edge hydrography on seasonal to decadal timescales, changes in the ocean-shelf geostrophic transport are subtle. This is due to a persistent large-scale steric sea surface slope along the shelf edge. The geostrophic flow induces local depth-integrated cross-isobath nitrate fluxes of O(1–10 mmol/m/s). This is similar in magnitude to the winter wind-driven nitrate transport, but is much less variable at seasonal and inter-annual time scales. Variability in the geostrophic advection of nitrate is thus determined by the ocean-shelf nitrate gradient's variability, rather than by the cross-isobath flow's variability. Geostrophic transport may therefore be an important baseline component of the nutrient and carbon budgets on the NWES and other continental shelves, and should be considered in their long-term response to climate-scale forcing.

Plain Language Summary Deep ocean waters typically contain high concentrations of nutrients (such as nitrate) that marine algae, plants at the base of the marine ecosystem, need to grow. On the North West European Shelf (NWES), these nutrient-rich waters originate far away from the coast, but are brought to shallower regions by subtle ocean flows much weaker than strong currents like the Gulf Stream. We study a particular transport mechanism associated with gentle slopes in the sea surface that exist along the NWES edge, which, due to the Earth's rotation, produce ocean currents across the NWES edge (i.e., toward the coast or away from it). We find that although these currents move at just a few centimeters per second, they are remarkably persistent across different seasons, years, and decades, and can therefore have substantial impacts on marine ecosystems. Because they change so little in time, their effect on coastal nutrient concentrations in different regions of the NWES is determined by ocean-shelf contrasts in nutrient concentrations (rather than by the water flow itself). This subtle mechanism plays an important role in sustaining the NWES' ecosystem, and is likely relevant for understanding how other shelf seas function and respond to climate change.

1. Introduction

Physical and biogeochemical properties in the coastal ocean are strongly influenced by exchanges with the adjacent deep ocean. Despite accounting for only ≈7% of the global ocean's surface area (e.g., Simpson & Sharples, 2012), continental shelves are major contributors to atmospheric carbon dioxide sequestration, particulate carbon export, and other fluxes in the global carbon cycle (Roobaert et al., 2024, and references therein). Further, most of the dissolved nitrogen that fuels new primary production in the coastal ocean originates from the deep ocean (Liu et al., 2010). The ecosystems sustained by this shelf sea primary production provide >90% of global commercial fisheries (Pauly et al., 2002; Stock et al., 2017), as well as being an integral part of other sectors of the blue economy and coastal livelihoods across the global coastal ocean.

In the North West European Shelf (NWES), oceanic water masses originating from the North East North Atlantic are often found on the shelf (e.g., Graham et al., 2018; Porter et al., 2018; Huthnance et al., 2022; Wei et al., 2024). These nutrient-rich oceanic waters support primary production, and have been observed to be associated with elevated surface chlorophyll-a concentrations (e.g., Porter et al., 2018, their Figure 2). As a result, oceanic

intrusions also contribute to the NWES' carbon budget, which mediates atmospheric CO_2 drawdown, particulate carbon burial, and carbon export to the adjacent deep ocean (e.g., Wakelin et al., 2012; Legge et al., 2020).

These oceanic water intrusions are often driven by a combination of physical mechanisms, rather than by a single mechanism. The NWES is a case in point, where surface and bottom Ekman transports, barotropic tides, internal tides, high-frequency internal waves, mesoscale eddies/meanders, and interaction between the along-isobath geostrophic flow and irregular topography are all known to be relevant (Huthnance et al., 2022). Their importance for nitrate transport depends on the shelf edge segment being considered. For example, winter wind-driven Ekman transport is off-shelf in the Celtic Sea and Armorican Shelf, and on-shelf farther north (Wei et al., 2024, hereafter W24). Higher-frequency processes such as internal tides and nonlinear internal waves have been observed in particular locations (Huthnance et al., 2022; Moncuquet et al., 2025; Spingys et al., 2020). However, the contributions of these processes to cross-shelf volume or nutrient transport in a shelf-wide sense are unknown. Considering this complex combination of exchange processes, it is also unclear what will drive variability in the NWES' circulation and biogeochemical cycles in a changing climate.

Imprints of climate-scale changes in North Atlantic circulation and water masses could have important effects. Warmer and more saline waters of subtropical origin have had an increased presence in the Rockall Trough in recent decades (a phenomenon sometimes called "subtropicalization", e.g., Clark et al., 2022), resulting in modified shelf-edge circulation and inflows into the North Sea (Marsh et al., 2017). These inflows may weaken significantly by 2100, making the North Sea stagnant and more vulnerable to eutrophication and hypoxia (Holt et al., 2018). Another large-scale change observed along the NWES edge happened in the mid-2010s, when a major low-salinity anomaly formed in the North Atlantic due to anomalous wind-driven Subpolar Gyre circulation (Holliday et al., 2020).

In this work, we examine and quantify geostrophic ocean-shelf transport across the NWES edge at seasonal and decadal timescales, using historical in situ hydrographic data, climatologies, and satellite-derived sea surface height measurements. We find the presence of persistent, large-scale along-isobath pressure gradients linked to sea surface slopes, which support cross-isobath geostrophic transports associated with important ocean-shelf nutrient fluxes. We first describe our data sets and analysis methods in Section 2, and present results in Section 3. In Section 4, we discuss the broader significance of our results in the context of ocean-shelf transport on the NWES, and conclude with a summary of our findings in Section 5.

2. Data Sets and Methods

To quantify geostrophic ocean-shelf transports, we analyze variability along the 200 m isobath (the NWES edge). To compare our results with W24's, we divide the NWES edge into six segments following their definition (Figure 1a): Armorican Shelf (AS), Celtic Sea Shelf (CSS), Porcupine Sea Bight Shelf (PSBS), Malin Shelf (MS), Hebrides Shelf (HS), and West Shetland Shelf (WSS). We also add a further segment to the east (North East North Sea Shelf, NENSS), along the southern rim of the Norwegian Trench.

2.1. Objectively-Mapped Climatologies

We use 1/4° gridded fields (1° for nitrate) from the World Ocean Atlas 2023 climatology (objectively-mapped following Levitus et al., 2012) to examine the along-shelf distribution of temperature (Locarnini et al., 2024), salinity (Reagan et al., 2024), nitrate (Garcia et al., 2024), and geostrophic cross-isobath transports. We derive Conservative Temperature Θ, Absolute Salinity S_A and potential density anomaly σ_0 using the Thermodynamic Equation of State for Seawater (TEOS-10). The geographic correction to S_A has weak spatial variability and hence negligible effects on density gradients. We then interpolate these fields to the 200 m isobath contour extracted from version 2.7 of the SRTM15+ data set (IGPP, 2025; Tozer et al., 2019) and smoothed with a 75 km running mean in the along-isobath direction to filter out small-scale topographic features unresolved by the WOA23 fields. We use the WOA23 seasonal averages and decadal/near-decadal averages (1975–1984, 1985–1994, 1995–2004, 2005–2014 and 2015–2022). Nitrate measurements are even more sparse than temperature and salinity measurements (Figure S1 in Supporting Information S1), and the mapped nitrate fields are only available as seasonal averages. We therefore do not examine the decadal variability of the shelf-edge nitrate distribution and its cross-isobath transports. Mapped fields are available at the standard WOA vertical levels, with vertical spacing varying from 5 m near the surface to 25 m at the 200 m depth level (the shelf edge isobath). All fields are interpolated to a uniform 5 m vertical grid. Figure 1a shows the potential density distribution at 200 m depth.

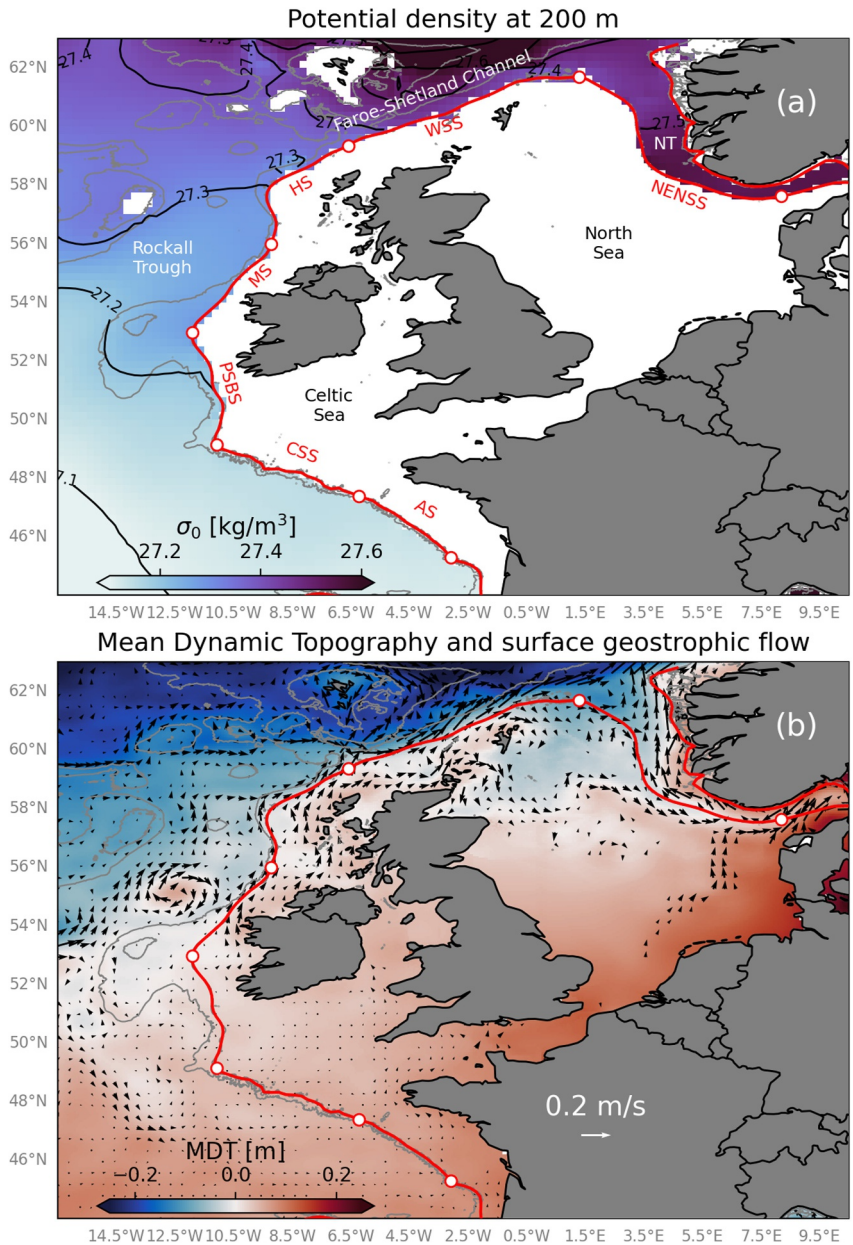

Figure 1. Time-mean density structure and surface geostrophic flow on the NWES. (a) Potential density at 200 m depth from the WOA23 climatology. (b) Mean Dynamic Topography from the regional 1/16° Copernicus Marine Environment Monitoring Service product and surface absolute geostrophic velocity vectors. Vectors with magnitude smaller than the local interpolation error are masked out. Gray lines are the 200 and 1000 m isobaths, and the thick red line is the smoothed 200 m isobath used in the shelf-edge analyses. AS = Armorican Shelf, CSS = Celtic Sea Shelf, PSBS = Porcupine Sea Bight Shelf, MS = Malin Shelf, HS = Hebrides Shelf, WSS = West Shetland Shelf, NENSS = North East North Sea Shelf, NT = Norwegian Trench.

To better constrain nitrate concentrations on the shelf, we use the annual (1960–2014) North Sea Biogeochemical Climatology (NSBC, Hinrichs et al., 2017). The data set covers most of the NWES (except for the Armorican Shelf segment in the south), and is based on quality-controlled temperature, salinity, and biogeochemical measurements in the 1960–2014 period derived from eight data sources. The climatology has a 1/4° lateral resolution and 22 vertical levels with variable vertical spacing (5 m near the surface and 32 m near 200 m). The NSBC fields include monthly seasonal averages and the 1960–2014 long-term mean, both in bin-averaged (Level 2, Figure S2 in Supporting Information S1) and objectively-mapped (Level 3) formats. Following W24, we focus on the Level

2 data for seasonal estimates of nitrate concentrations on the shelf to avoid mapping artifacts in data-sparse areas of the NWES.

2.2. Bin-Averaged Shelf-Edge Climatology

We supplement our time-averaged analyses with a new along-isobath climatology constructed following a method based on Jones et al. (2023). This is done to refine the shelf-edge analysis and assess the effects of isotropic spatial smoothing associated with WOA23's objective mapping scheme. The main quality-controlling steps involve a local range test (any measurements outside of a 5 standard deviation envelope at each depth level are rejected) and a density inversion test (any profiles with density inversions greater than 0.03 kg/m^3 over 20 dbar are rejected). For details, see Jones et al. (2023, their Figure S2).

To construct the gridded fields, we search for all quality-controlled temperature and salinity profiles in the EN4 data set (Good et al., 2013) found inside a running isobath-following polygon, for each point along the 200 m isobath spaced in 20 km steps. To account for the anisotropy of topography-following flow, the polygon is 100 km long in the along-isobath direction and 10 km wide in the cross-isobath direction (8 km offshore and 2 km inshore of the 200 m isobath). The cross-isobath asymmetry of the polygon is based on typical inshore (<5 km) and offshore (≈10 km) first surface deformation radii on the NWES (LaCasce & Groeskamp, 2020, their Figure 8) and observed Slope Current cross-isobath scales (Fraser et al., 2022, their Figure 6). Where there are less than 5 valid profiles within the polygon, the along-isobath length is increased in 50 km increments (up to 300 km) until at least 5 profiles are found. The profiles are then density-sorted to remove density inversions associated with intense turbulence at the shelf edge, and the shallowest valid data point between 10 m and the surface is repeated up to 0 m. The profiles are then distance-weighted using a Gaussian function to prevent spatial biasing by isolated segments with denser data coverage.

2.3. Satellite Altimetry

To examine the sea level distribution along the shelf edge and to reference cross-isobath baroclinic transports, we use the regional Mean Dynamic Topography (MDT, CMEMS, 2024b) and Absolute Dynamic Topography (ADT, CMEMS, 2024a) products for the European seas distributed by the CMEMS. These Level 4 multi-satellite MDT/ADT products apply tidal corrections and Dynamic Atmospheric Correction steps that include filtering out high-frequency (periods <20 days) barotropic wind-driven signals, and static atmospheric pressure loading (i.e., the inverted barometer effect). The MDT and ADT maps are constructed based on the calibration and objective mapping procedure described in Pujol et al. (2016). The data sets are provided on a $1/16°$ grid covering the NWES in the 1993–2024 period. The MDT (Figure 1b) is a 1993–2012 average that has shown good agreement with independent in situ measurements with a ≈20 km spectral noise floor (CMEMS, 2024b), significantly finer than the ≈100 km effective resolution found in global L4 ADT products (Ballarotta et al., 2019). The MDT and ADT are respectively associated with the time-mean and time-varying surface geostrophic circulation.

2.4. Diagnostic Quantities

To examine the seasonal variability in the density structure and whether it has an effect on the cross-isobath transports, we use metrics for the along-isobath stratification (depth-integrated density gradient magnitude) and vertical stratification (Potential Energy Anomaly (PEA)). We also decompose the sea surface height into density (steric) and mass (manometric) change components to determine whether the along-isobath pressure gradients (and the associated cross-isobath geostrophic flow) are related to changes in local shelf stratification or advective changes (e.g., Wise et al., 2024). We detail these diagnostic metrics below.

2.4.1. Stratification

Defining (x, y, z) respectively as the cross-isobath, along-isobath, and vertical coordinates, we quantify the time-mean shelf edge stratification and its seasonal cycle using two metrics: For the geostrophically-balanced cross-isobath flow's magnitude, we use the depth-averaged along-isobath density gradient magnitude $|\partial_y \rho|$, and for the water column's vertical stratification, we use a form of the PEA (e.g., Simpson & Bowers, 1981) based on the depth-averaged potential density, that is,

$$\mathrm{PEA}(y) = -\frac{g}{h}\int_{-h}^{0} z[\rho(S_A,\Theta) - \overline{\rho}(S_A,\Theta)]\, dz, \tag{1}$$

where g is gravity, $h = 200$ m is the bottom depth, $\rho(y,z)$ is density, S_A is Absolute Salinity, and Θ is Conservative Temperature, and $\overline{\rho}$ is the depth-averaged density. The PEA quantifies the amount of work necessary to homogenize a stratified water column locally, and is a useful diagnostic for shelf vertical stratification. It has been estimated in regions of the NWES from observations and model fields (e.g., Holt & Proctor, 2008; Jones et al., 2018; Holt et al., 2022).

2.4.2. Steric Sea Surface Height

We compare the total sea level measured by satellite altimetry with the sea surface height due to density (steric) effects. The steric contribution to sea level can be estimated by starting from hydrostatic balance, that is,

$$\partial_z p = -g(\rho_0 + \rho'), \tag{2}$$

where p is pressure, and $\rho'(y,z) \equiv \rho(y,z) - \rho_0$ is a perturbation density relative to $\rho_0 = 1027.5$ kg/m^3 (a Boussinesq reference density). Integrating Equation 2 from the bottom $z = -h = -200$ m to the surface $z = \eta(y)$ and neglecting the small term $\int_0^\eta \rho'/\rho_0\, dz$ gives the following expression for η (e.g., Wang et al., 2018):

$$\eta(y) = \underbrace{\frac{p_b' - p_a}{g\rho_0}}_{\eta_m} \underbrace{- \frac{1}{\rho_0}\int_{-h}^{0} \rho'\, dz}_{\eta_s}, \tag{3}$$

where p_a is the surface (atmospheric) pressure and $p_b' = p_b - g\rho_0 h$ is the bottom pressure perturbation. Equation 3 splits the total sea level η into a dynamic manometric component η_m, associated with mass loading from the combined water and air columns (see Piecuch et al., 2022, for details), and a steric component η_s, associated with the depth-integrated density structure.

3. Geostrophic Transport Across the Shelf Edge

In this section, we analyze the along-isobath and temporal variability of the geostrophic transport across the NWES shelf edge and the mechanisms maintaining it. We begin by examining the time-averaged (1975–2024) and seasonal shelf-edge hydrography, cross-isobath geostrophic transport and its relation to the along-isobath sea surface height structure in Section 3.1, as well as the associated ocean-shelf nitrate fluxes in Section 3.2. We then examine decadal variability of the geostrophic transport in Section 3.3.

3.1. Seasonal Stratification and Cross-Isobath Geostrophic Flow

The hydrography at the NWES edge has important along-isobath gradients. From the southern Armorican Shelf (segment 1) to the northern West Shetland Shelf (segment 6), warm and saline Eastern North Atlantic Water (ENAW) originating from the adjacent deep ocean occupies the shelf edge (e.g., W24 and Figures 2f, 2k, and 2p). ENAW has been observed on the Malin Shelf, transported onshore by the Atlantic Inflow Current (Porter et al., 2018). A hint of this intrusion pathway seems to be visible in the mean surface geostrophic circulation (Figure 1b at 56°N, 9°W). East of Shetland, fresher water influenced by mixing with the Baltic Outflow (BO) is found along the edge of the North East North Sea Shelf (NENSS, segment 7), along the southern rim of the Norwegian Trench.

This mean shelf-edge stratification has pronounced seasonal variability (e.g., Holt & Proctor, 2008; Ruiz-Castillo et al., 2019; Figures 2f–2y). Strong wintertime surface heat loss and winds nearly homogenize the water column along most of the shelf edge's extent (Figure 2, second column). In the summer, a developed pycnocline in the upper ≈100 m exists (Figure 2, fourth column), with onset and erosion in the spring and autumn, respectively (Figure 2, third and fifth columns). But despite these seasonal changes in vertical stratification, robust along-isobath density gradients persist, both in the annual average and across all seasons. Less dense water is present toward the south, especially south of the Rockall Trough (off of the AS and CSS edge) and toward the

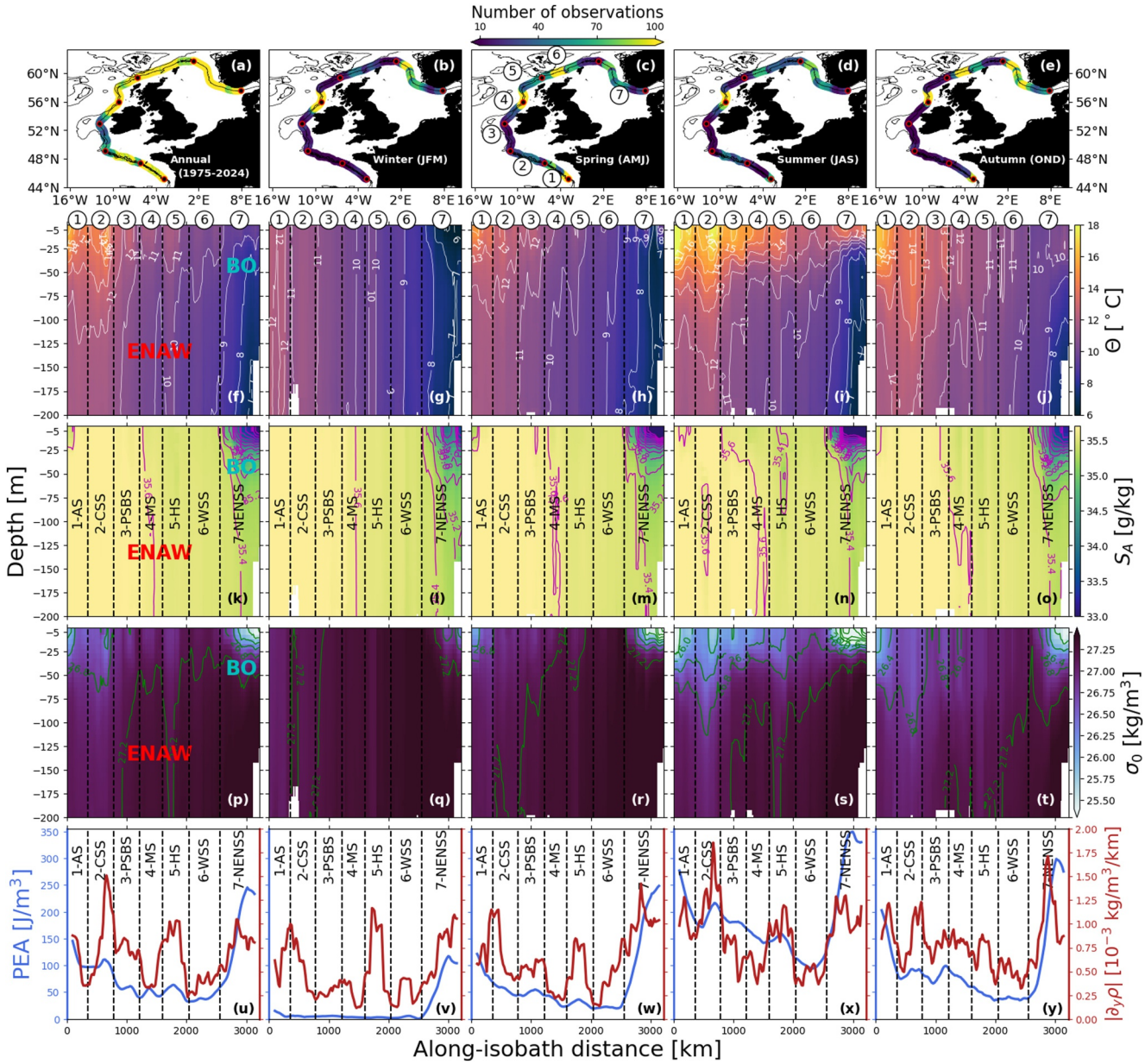

Figure 2. Time-mean and seasonal hydrographic variability along the NWES edge from the bin-averaged shelf-edge climatology. (a–e) Vertical mean of valid EN4 data points used in each along-isobath bin. Gray lines are the 200 and 1000 m isobaths. (f–j) Conservative Temperature Θ, (k–o) Absolute Salinity S_A, (p–t) potential density anomaly σ_0, and (u–y) Potential Energy Anomaly and vertically-averaged along-isobath density gradient magnitude $|\partial_y \rho|$, smoothed with a 200 km-wide running mean. The columns respectively group, from left to right, the annual mean (1975–2024), winter, spring, summer, and autumn climatological fields. Vertical dashed lines are the segment boundaries indicated as black dots on panels (a–e), and enumerated 1–7 on panel (c). ENAW = Eastern North Atlantic Water, BO = Baltic Overflow.

northeast, just offshore of the NENSS edge. Between these two density minima, denser water occupies the shelf edge adjacent to the Faroe-Shetland Channel and the WSS edge (Figures 1a and 2p–2t).

The 1975–2024 time-mean bulk vertical stratification (quantified by the PEA, Equation 1) in the warmer southern segments (1, 2) and in the fresher NENSS (7) is 2–5 times stronger than in the central section of the shelf edge (segments 3–6, Figure 2u). The PEA values are consistent with other observational estimates on the NWES (Holt et al., 2022; Jones et al., 2018). The along-isobath lateral density gradient magnitudes $|\partial_y \rho|$ vary by similar amounts, but on shorter scales. Importantly, while the shelf edge-averaged PEA increases by a factor of 11 from winter to summer, $|\partial_y \rho|$ is more persistent, changing only by a factor of 1.8 (Figures 2v–2y). So while the only

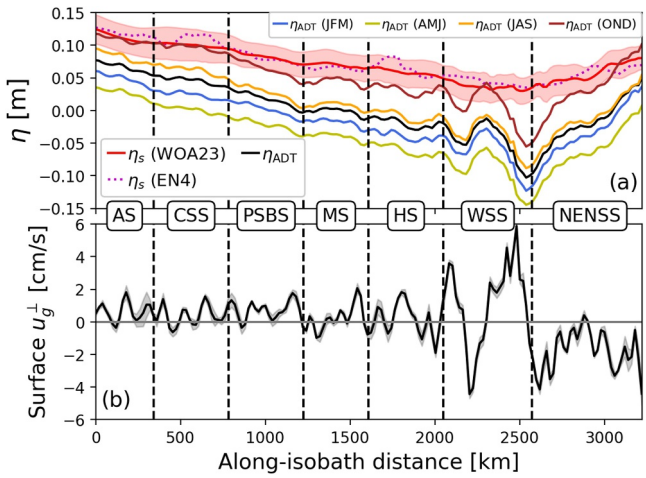

Figure 3. Seasonal sea surface height and surface geostrophic velocity along the NWES edge. (a) Satellite-derived time-averaged Absolute Dynamic Topography η_{ADT} (seasonal and annual averages) and steric height η_s, derived from the EN4 along-isobath climatology (dotted magenta line) and from WOA23 (red line, shading indicates ±1 standard deviation about the time mean). (b) Surface geostrophic cross-isobath velocity (positive onshore) associated with η_{ADT} (shading indicates ±1 standard deviation about the time mean).

permanently vertically-stratified segment is the NENSS, thermal wind-balanced cross-isobath flow is present year-round in all segments.

The low and high density shelf edge regions are collocated with high and low mean sea level, respectively (Figure 1b), suggesting that much of the mean sea level variability along the shelf edge is steric (see also Wise et al., 2024). Figure 3a compares the 1993–2024 time-mean η_{ADT} from satellite altimetry with the η_s derived from the new EN4-based shelf-edge climatology (Figure 2p) and the WOA23 climatology. For the time-mean fields, the squared correlation coefficient between $\eta_{ADT}(y)$ and $\eta_s(y)$ derived from the EN4 (WOA23) climatology is 0.83 (0.90), indicating that the large-scale sea level structure along the shelf edge is mostly determined by along-isobath steric variations rather than by the manometric component known to be dominant in a shelf-averaged sense (Wise et al., 2024). The EN4-based η_s is bin-averaged, and thus includes smaller-scale structure than the WOA23-and ADT-based fields. The WOA23-derived η_s has higher correlation with the ADT because both fields were constructed with objective mapping techniques, thus filtering smaller spatial scales (Ballarotta et al., 2019; Levitus et al., 2012). While they miss smaller-scale along-isobath structure, the EN4 profile density is too low to support finer resolutions everywhere, and finer resolutions would approach the time-mean local deformation radius in some segments. We therefore use the WOA23 along-isobath fields to better combine the hydrographic and altimetric fields to derive geostrophic velocities. The absolute geostrophic cross-isobath velocity $u_g^\perp(y,z)$ can be diagnosed from the along-isobath density and sea level structures:

$$u_g^\perp(y,z) = \underbrace{\frac{1}{f}\partial_y \Phi_s}_{u_{gbc}^\perp(y,z)} + u_{g0}^\perp(y), \tag{4}$$

where f is the Coriolis parameter, $\Phi_s = \int_0^p \delta\, dp$ is the surface-referenced geopotential anomaly due to the water column's density structure (with δ being the specific volume anomaly calculated with the TEOS-10), and $u_{gbc}^\perp(y,z)$ is the baroclinic cross-isobath velocity relative to the sea surface. The surface geostrophic velocity $u_{g0}^\perp \equiv -\frac{g}{f}\partial_y \eta_{ADT}$ (shown in Figure 3b) is derived from the ADT. The large-scale flow is generally on-shelf between the AS and the WSS and off-shelf in the NENSS with several local reversals. Importantly, along-isobath gradients in η are remarkably persistent year-round, making $u_{g0}^\perp$ very steady. The along-isobath median of the $u_{g0}^\perp$ standard deviation is 0.27 cm/s, significantly smaller than the O(1 cm/s) mean amplitudes in most along-isobath locations. The WSS has localized larger on-shelf/off-shelf geostrophic velocities of up to 6 cm/s. Rather than developing localized slopes during particular seasons, the entire sea surface structure "breathes" up and down preserving a coherent along-isobath structure (Figure 3a). This picture is consistent with dominant modes of shelf-wide sea level variability in the NWES (Diabaté et al., 2025; Wise et al., 2024).

Figures 4a–4e show the cross-isobath geostrophic flow's vertical structure. Like the surface flow, it has weak seasonal variability and is mostly onshore from the AS to the WSS and offshore in the NENSS, with magnitudes of O(1 cm/s). It also has little vertical shear, with the amplitude of the absolute geostrophic velocity $u_g^\perp$ being typically 2–10 times greater than the baroclinic geostrophic velocity relative to the surface, $u_{gbc}^\perp$. Some vertical structure in $u_{gbc}^\perp$ develops near the surface over the spring/summer with the pycnocline's formation and enhanced freshening of the NENSS. This causes a modest increase in the offshore velocity in the NENSS and a similar increase in the onshore velocity elsewhere (Figures 4c and 4d). But these seasonal departures from the annual mean are small (Figures 4b–4e, the medians of the seasonal anomalies' absolute values are ≤0.1 cm/s), suggesting that the sea surface height variability measured with satellite altimetry gives a good proxy for the depth-integrated cross-isobath transport's structure along the NWES edge.

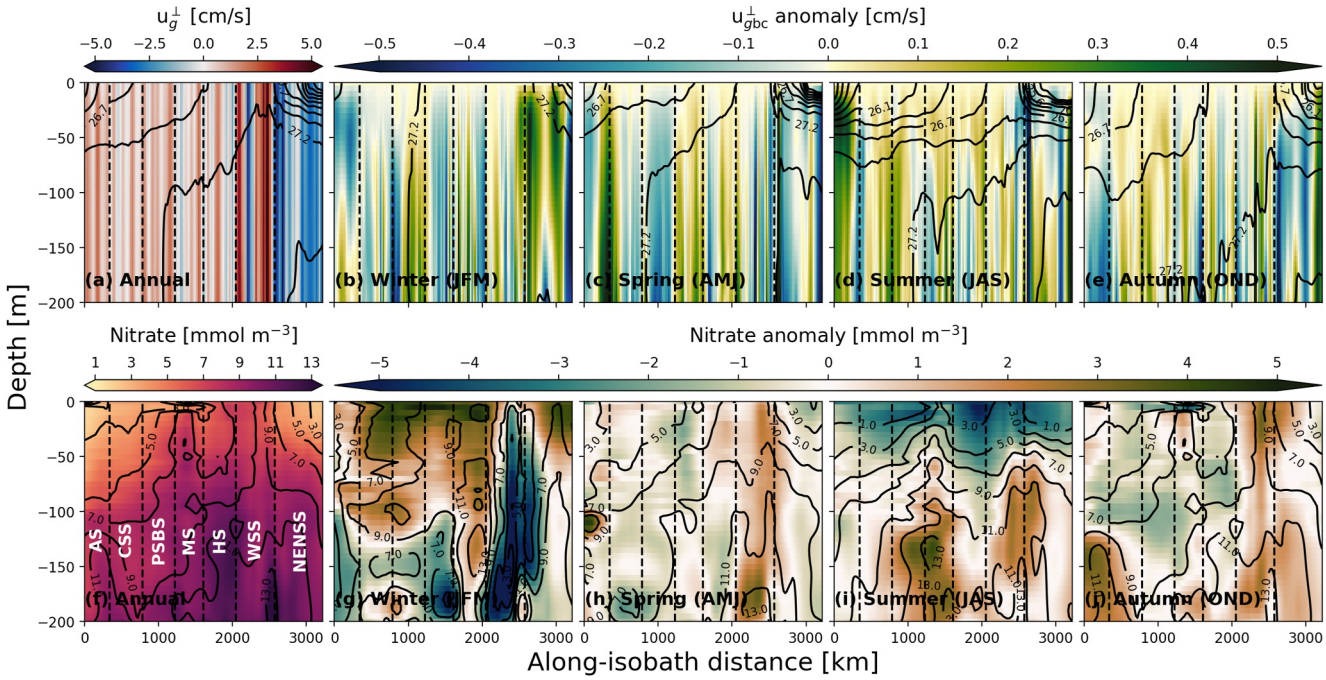

Figure 4. Vertical structure of cross-isobath geostrophic velocity (a–e) and nitrate concentration (f–j) along the NWES edge. (a) Time-mean absolute geostrophic velocity $u_g^{\perp}$ (positive onshore). (b–e) Seasonal anomalies of the baroclinic geostrophic velocity, $u_{gbc}^{\perp}$, relative to its annual mean. (f) Time-mean nitrate concentration. (g–j) Seasonal nitrate concentration anomalies. In panels (a–e), the black contours are isopycnals, while in panels (f–j) they indicate nitrate concentrations.

3.2. Ocean-Shelf Geostrophic Nitrate Transport

The shelf-edge nitrate concentration has a more complex structure (Figures 4f–4j). Mean nitrate values near the surface are low, ≈3 mmol/m^3 toward the south (AS/CSS) and northeast (NENSS) ends of the 200 m isobath, and about twice as large in between. Near the bottom, nitrate concentrations are higher, around 10 mmol/m^3. Concentrations also have significant seasonal variability, with a winter (summer) excess (deficit) of 1–5 mmol/m^3 relative to the annual mean. In the HS, the climatological nitrate concentration (≈10 mmol/m^3 in the winter and ≈5 mmol/m^3 in the summer) is consistent with high-resolution moored measurements taken in 2017–2018 (Johnson et al., 2024, their Figure 4b).

In a depth-averaged sense, shelf-edge annual-mean nitrate increases by ≈3 mmol/m^3 between the AS and WSS, with NENSS concentrations marginally lower (Figure 5a). Although the nitrate distribution along the shelf edge changes, the steadiness of the cross-isobath velocity's structure results in a persistent on-shelf/off-shelf nitrate transport pattern (Figures 5b and 5d). Depth-integrated nitrate transport averaged within segments is onshore between AS and WSS (ranging from 5.5 mmol/m/s to 27.4 mmol/m/s), and strongly offshore in the NENSS (−37.5 mmol/m/s), along the Norwegian Trench's southern rim. The seasonal standard deviations are everywhere O(1 mmol/m/s), emphasizing the persistence of this nitrate transport mechanism. The seasonal variation is more significant in the western NWES (PSBS, MS, HS, WSS) due to the smaller mean values (standard deviation ≈20%–40% of the mean value), and less significant in the AS, CSS, and NENSS (standard deviation ≈10% of the mean value).

The nitrate concentrations on the shelf, averaged between the 200 and 100 m isobaths (N_{shelf}) are mostly 1–5 mmol/m^3 lower than at the shelf edge (N_{ocean}), except for the WSS and NENSS in the winter (dashed lines in Figure 5a). This cross-shelf nitrate gradient is essential for an actual nitrate change on the shelf, since the strength of the ocean-shelf geostrophic transport $u_g^{\perp}$ is irrelevant if off-shelf and on-shelf nitrate concentrations are the same. We therefore quantify the depth-averaged nitrate transport convergence (across a typical cross-shelf distance L_x)

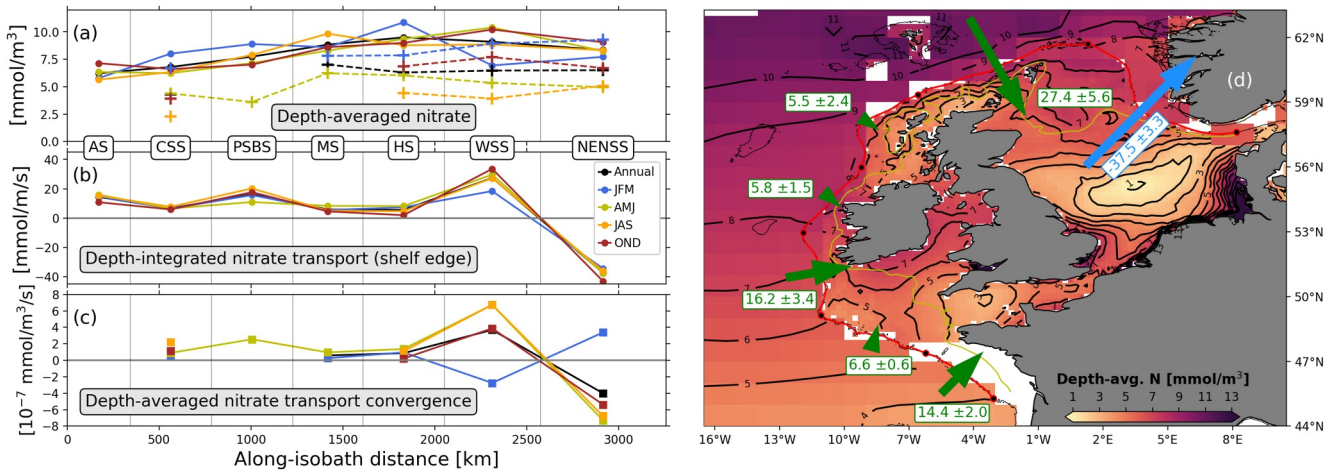

Figure 5. Nitrate concentration and ocean-shelf geostrophic transport averaged in different NWES segments. (a) Depth-averaged nitrate concentration, where solid lines are WOA23 averages along the 200 m isobath (N_{ocean}) and dashed lines are NSBC area-averages of all nitrate profiles between the 200 and 100 m isobaths within each segment (N_{shelf}). For N_{shelf}, profiles with depth-averaged salinity smaller than 34.5 are excluded, and spatial averages are only calculated for segments with more than 20 profiles available in a given season. (b) Depth-integrated cross-isobath geostrophic nitrate transport across the 200 m isobath (positive onshore). (c) Depth-averaged ocean-shelf nitrate transport convergence (positive means nitrate increase on the shelf). (d) Depth-averaged annual mean nitrate concentration between the surface and 200 m or the bottom, whichever is shallower (color scale and black contours). Nitrate concentrations are from WOA23 (NSBC) gridded fields offshore (inshore) of the 200 m isobath. The red (yellow) line is the 200 m (100 m) isobath. Shelf-edge depth-integrated nitrate transports (black line in panel (b)) are plotted as arrows (green onshore, blue offshore). The numbers shown in the boxes adjacent to the arrows are the annual mean ± the standard deviation, in mmol/m/s.

$$T_{\text{gN}} \equiv -\frac{1}{h}\int_{-h}^{0} u_g^{\perp} \times (N_{\text{shelf}} - N_{\text{ocean}})/L_x \, dz, \tag{5}$$

averaged within each segment in Figure 5c. We use $L_x = 100$ km as a representative distance between the 200 and 100 m isobaths (Figure 5d), and note that variations in L_x across segments may introduce factors of ≈1/2 to ≈ 2 in T_{gN}. Between the CSS and the HS, T_{gN} is positive in all seasons, varying between $0.2 - 2.7 \times 10^{-7}$ mmol/m^3/s. Without nitrate sinks such as biological uptake by phytoplankton, this nitrate flux would result in a volume-averaged concentration increase of 0.2–2.1 mmol/m^3 over 3 months. The magnitude of this variation is important, considering that the observed seasonal amplitude of the near-bottom nitrate concentration in the middle and outer shelf is ≈2–4 mmol/m^3 (Ruiz-Castillo et al., 2019, W24). For comparison, combining typical nitrate concentrations in the HS (Figure 5a) with eddy diffusivity coefficient estimates (Huthnance et al., 2022, their Table 10) yields diffusive nitrate flux convergence values that are an order of magnitude smaller than our geostrophic nitrate transport convergence estimates.

In the WSS (NENSS), the nitrate transport convergence T_{gN} increases to $\approx 6.7 \times 10^{-7}$ mmol/m^3/s ($\approx -6.8 \times 10^{-7}$ mmol/m^3/s) in the spring and summer. In both the WSS and the NENSS, the ocean-shelf nitrate gradient switches sign in the winter (shelf nitrate concentrations become ≈2 mmol/m^3 greater than offshore, Figure 5a), temporarily contributing to a nitrate decrease (increase) in the WSS (NENSS). The WSS and NENSS fluxes approximately cancel each other, but still impact the local shelf nitrate tendencies. While these fluxes are a reliable source/sink of nitrate, the redistribution of nitrate between different regions of the NWES depends on the details of the shelf circulation and biogeochemistry, which we are unable to examine with our data sets.

3.3. Interannually Persistent Cross-Isobath Geostrophic Flow

The seasonal cross-isobath flow patterns at the shelf edge (Figure 3b) are also found at longer timescales. Figure 6 shows decadal averages of the ADT η_{ADT} and the surface cross-isobath geostrophic flow $u_{g0}^{\perp}$. Similarly to the seasonal variability, $u_{g0}^{\perp}$ has been steady since the start of the altimetry record with decadal changes smaller than 1 cm/s, as the large-scale structure of η_{ADT} mostly preserves the along-isobath gradients associated with cross-isobath flow. Between 1995 and 2022, the along-isobath averaged η_{ADT} has risen at an average rate of 2.2 mm/year, close to the ≈3 mm/year trend observed in global mean sea level (e.g., Nerem et al., 2018;

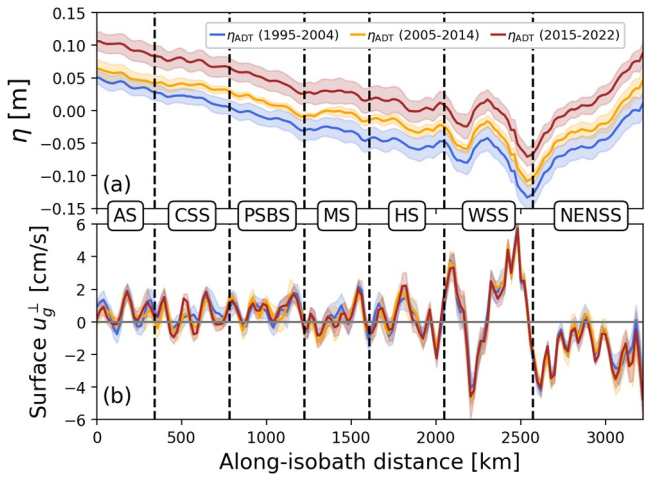

Figure 6. Decadally-averaged sea surface height and surface geostrophic velocity along the NWES edge. (a) Satellite-derived time-averaged Absolute Dynamic Topography (η_{ADT}). (b) Surface geostrophic cross-isobath velocity (positive onshore) associated with η_{ADT}. Shadings (panels (a, b)) indicate ±1 standard deviation about each decadal time mean.

Frederikse et al., 2020). In contrast, the steric component η_s (not shown) has risen only by 0.38 mm/year in the same period. This is a 17% contribution to the total NWES edge sea level change, significantly smaller than the globally-averaged estimates of 36% (Frederikse et al., 2020, their Table 1) or 56% (Nerem et al., 2018, their Table 2). So although the large-scale along-isobath sea surface height *gradients* are mostly determined by the steric component's spatial structure (Figure 3a), the along-isobath mean and its seasonal and decadal changes in recent decades have been controlled by NWES-wide mass changes, that is, the manometric component. This result is consistent with the finding that local and remote winds are important drivers of these mass fluctuations on monthly-to-decadal timescales (Diabaté et al., 2025; Wise et al., 2024), where the manometric component dominates over the steric component (Wise et al., 2024). The trend also reflects global mass inputs to the ocean.

Despite the steadiness in the shelf-edge sea-level gradients and geostrophic transport patterns, the NWES edge hydrography has experienced significant inter-decadal variability in the past five decades. Figure 7 shows decadal anomalies (1975–1984, 1985–1994, 1995–2004, 2005–2014, 2015–2022) of shelf-edge hydrography (Θ, S_A, σ_0) and baroclinic cross-isobath flow, $u_{gbc}^{\perp}$ relative to the 1975–2022 mean. Since the late 1990s, the NWES edge has seen strong warming (likely associated with a greater presence of subtropical waters in the Rockall Trough, e.g., Clark et al., 2022), with associated salinification between 1995 and 2014. The 2015-2022 decade, on the other hand, shows the imprint of a major low salinity event that originated in the Subpolar North Atlantic in the mid-2010s (Holliday et al., 2020) and was observed in the northern Rockall Trough around 2017 (Fraser et al., 2022). However, the density change caused by this event is very uniform along the shelf edge (Figure 7o), and the magnitude of the associated $u_{gbc}^{\perp}$ changes (<0.5 cm/s, Figure 7t) is similar to the magnitude of seasonal anomalies (Figures 4b–4e) and to the surface $u_g^{\perp}$ decadal variations observed in the altimetry era (Figure 6b). The decadal $u_{gbc}^{\perp}$ anomalies since 1975 (Figures 7p–7t) are generally not strong enough to cancel the time-mean geostrophic flow locally (Figure 4a).

This picture suggests that the imprint of large-scale Subpolar North Atlantic changes on the cross-isobath geostrophic flow may be less significant than the variations in the ocean-shelf nitrate gradients (Figure 5) for the convergence of ocean-shelf transports and temporal changes in shelf nitrate levels. Deep-ocean nitrate concentrations adjacent to the NWES edge show interannual variations of 1–2 mmol/m^3 in the western and northern segments (from PSBS to NENSS) and up to 4–5 mmol/m^3 in the southern segments AS and CSS (see W24's Figure 5 and Section 1). This should be taken as speculative though, as there do not seem to be published estimates of the ocean-shelf nitrate *gradient* variability at interannual and longer timescales.

4. Discussion

In the following, we compare our geostrophic transport estimates in the NWES to previous results on wind-driven nitrate transports and discuss their implications in a broader context in Section 4.1. We then discuss the reasons for the persistent signature of geostrophic cross-isobath transport in Section 4.2, consider the potential relevance of the process to other regions in Section 4.3, and discuss the limitations involved in our analysis in Section 4.4.

4.1. Geostrophic and Wind-Driven Ocean-Shelf Transport Mechanisms

While the geostrophic cross-isobath flow represents a reliable on-shelf nitrate transport mechanism across most of the NWES, the wind-driven circulation is more variable. The time-mean winds are downwelling-favorable, with onshore (offshore) surface (bottom) Ekman transport north of the CSS. When combined with deep mixed layers extending below the shelf edge's depth in late winter, the on-shelf Ekman transport is a source of nitrate for the shelf (W24). The AS and CSS segments tend to have more upwelling-favorable winds (e.g., Graham et al., 2018; Huthnance et al., 2022), resulting in offshore winter nitrate Ekman transport (W24).

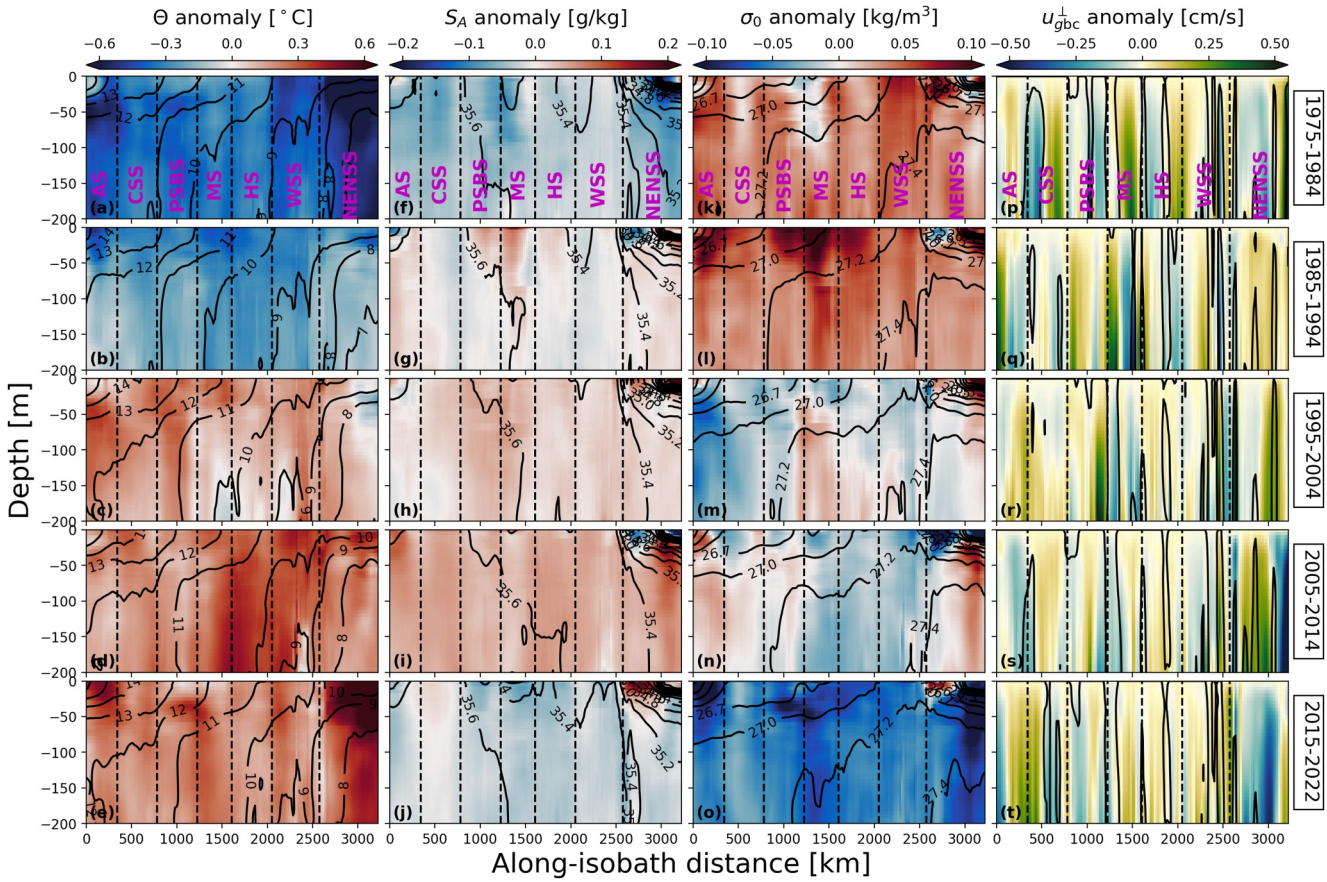

Figure 7. Decadal variability along the NWES edge. (a–e) Conservative Temperature Θ, (f–j) Absolute Salinity S_A, (k–o) potential density anomaly σ_0, and baroclinic geostrophic velocity $u^{\perp}_{gbc}$ (p–t). The color scale in each row is the decadal anomaly relative to the long-term (1975–2022) mean. The black contours overlaid are the Θ, S_A, σ_0, and $u^{\perp}_{gbc}$ values for each decade. In panels (p–t), only the $u^{\perp}_{gbc} = 0$ contour is plotted.

It is therefore useful to compare our winter geostrophic transport estimates with W24's wind-driven Ekman transport estimates (Table 1). W24 find off-shelf wind-driven nitrate transports of −3.7 mmol/m/s and −5.4 mmol/m/s in the AS and CSS, respectively. The winter onshore geostrophic transports (14.8 mmol/m/s and 6.4 mmol/m/s) compensate part of this off-shelf flow, making the combined (geostrophic + wind-driven) nitrate transport on-shelf. The geostrophic transport in the south is also on-shelf during the rest of the year, and the cross-shelf nitrate gradient is negative (Figure 5). The combined mechanisms thus represent an annually-averaged source of nitrate for the southern NWES. From the PSBS to the HS, both processes are associated with on-shelf, convergent nitrate transports, thus also representing a nitrate source for the western NWES. This is also the case in the WSS between spring and autumn, but the ocean-shelf nitrate gradient switches sign in the winter (Figures 5a–5c). This creates a net nitrate sink for the WSS during the winter. In the NENSS, The sea surface slopes upward toward the Baltic Sea, sustaining off-shelf geostrophic flow (Figures 3 and 6). This removes nitrate from the shelf between spring and autumn (when the ocean-shelf nitrate gradient is negative), but that process reverses during the winter (Figures 5a–5c). To our knowledge, cross-isobath wind-driven nitrate transport estimates are not available for the NENSS edge.

Table 1
Comparison Between NWES Segment-Averaged Winter Wind-Driven and Geostrophic Nitrate Transports, in mmol/m/s (Positive on-Shelf)

Segment	Wind-driven[a]	Geostrophic	Combined
AS	−3.7	14.8	11.1
CSS	−5.4	6.4	1.0
PSBS	1.1	15.7	16.8
MS	13.1	5.4	18.5
HS	6.9	7.3	14.2
WSS	6.6	18.4	25.0
NENSS	–	−34.5	-

[a]From Wei et al. (2024)'s Figure 7a.

A key distinction between the two mechanisms is that shelf-edge surface Ekman transport is a strongly seasonal nitrate delivery mechanism that depends on wintertime deep mixed layers and strong winds, while the geostrophic transports are present year-round. The dominant source of

seasonal variability in NWES geostrophic ocean-shelf nitrate exchange is thus the cross-shelf nitrate gradient (Figures 4b–4e, 5a, and 5c). At interannual timescales, W24 find significant variation in shelf-edge nitrate concentrations, as well as in wind-driven Ekman volume and nitrate transports (especially in the southern segments, their Figures 5 and 6). Future changes in wind patterns and storminess in the Eastern North Atlantic and the NWES could have impacts on the wind-driven nitrate recharge through changes in the on-shelf volume transport, the winter mixed layer depth, or both (W24).

In a more eutrophic NWES, ocean-shelf nitrate gradients might weaken or even reverse. While there are insufficient nitrate measurements to estimate the ocean-shelf nitrate gradient variability at decadal timescales, the sensitivity of geostrophic nitrate transport convergence to the cross-shelf nitrate gradient means that ocean-shelf geostrophic nitrate transport (and potentially other mechanisms) might weaken in future climates. This is a possible scenario for the North Sea, which is projected to become significantly more stagnant, hypoxic, and eutrophic by 2100 under some future climate scenarios. This possible regime shift is linked to a weakened geostrophic ocean-shelf volume transport caused by the presence of fresher North Atlantic waters and associated changes in the topographically-steered geostrophic NWES edge circulation (Holt et al., 2018).

From a modeling perspective, low-frequency cross-isobath geostrophic transports should be relatively computationally affordable to simulate, as the scales involved do not require eddy-resolving resolutions. However, the versions of the Atlantic Margin Model with 7 and 1.5 km horizontal resolution (AMM7 and AMM15, respectively) show differences in the interior cross-isobath transport (part of which is geostrophic) that can be partly attributed to AMM15's improved representation of stratification, bathymetry, and the European Slope Current, which influence the magnitude and position of shelf-edge pressure gradients (Graham et al., 2018).

There is also the possibility of change in deep-ocean nitrate concentrations. Biogeochemical North Atlantic simulations suggest a potential decrease of ≈1–4 mmol/m^3 in annual maximum nitrate concentrations at the NWES edge by the 2090s (Kelly et al., 2025, their Figure 3h). This emphasizes the need to understand both biogeochemical and circulation changes to predict the effects of deep-ocean imprints of North Atlantic variability on the NWES's carbon pump at climate scales, as it depends on nitrate primarily sourced from the adjacent deep ocean.

4.2. Why Is the Ocean-Shelf Geostrophic Transport so Persistent?

The remarkable persistence of cross-isobath geostrophic transport patterns along the NWES edge is linked to steady along-isobath sea surface gradients (Figures 3 and 6). Although the mean along-isobath structure of the sea surface is mostly steric (Figure 3a), its temporal changes along the shelf edge and on the shelf follow large-scale modes of variability, controlled both locally by Ekman volume transport convergence on the NWES and remotely via perturbations originating upwave of the NWES, along the Portuguese coast (Calafat et al., 2012; Diabaté et al., 2025; Wise et al., 2024). These signals are transmitted quickly along the boundary by Kelvin and coastal-trapped wave modes with phase speeds O(1 m/s), and thus take O(10 days) or less to cover the entire extent of the NWES edge (e.g., Hughes et al., 2019). These short time scales are consistent with the observed along-isobath uniformity of seasonal and inter-annual sea surface height variations, as the adjustment process largely preserves the along-isobath gradients (and hence the cross-shelf geostrophic flow) at these time scales.

4.3. Ocean-Shelf Geostrophic Nitrate Transport in Other Regions

It is useful to consider whether ocean-shelf geostrophic nutrient transport might also be important in other regions. Classical eastern boundary systems with large-scale alongshore pressure gradients such as the California Current System (e.g., Connolly et al., 2014) are likely candidates, and the geostrophic flow may complement the seasonal wind-driven upwelling. Western boundary current systems also have large-scale meridional baroclinic pressure gradients that sustain cross-isobath and vertical transport (Liao et al., 2022). In a western boundary shelf (South China Sea) decadal variability of the cross-isobath geostrophic transport has been attributed to the along-isobath pressure gradient's variations in response to El Niño-Southern Oscillation-related forcing (Song et al., 2025). A primary knowledge gap appears to be the implications of these cross-isobath flows for nitrate fluxes, especially on interannual and longer timescales. Our NWES results show that even modest cross-isobath flow can result in important nitrate input for the continental shelf, suggesting that this nutrient supply mechanism should be investigated in other regions.

4.4. Limitations

The main limitation of this work comes from the sparsity of available observations. The climatological fields (WOA23 hydrography and gridded satellite altimetry) are constructed using objective-mapping techniques that tend to smooth spatial variability. However, since along-isobath decorrelation scales are much longer than cross-isobath scales on the shelf (e.g., Brink, 2023), along-isobath structure can be estimated with greater accuracy than cross-isobath structure, considering the same sparse data distribution. The fact that the bespoke bin-averaged EN4 climatology captures the same large-scale along-isobath features as the objectively-mapped climatologies (Figure 3a) gives confidence in this approximation, but some cross-isobath variability could still remain in the along-isobath distributions. The coverage of the historical nitrate measurements (Figures S1 and S2 in Supporting Information S1) also limits analysis of the temporal nitrate variability beyond seasonal means (see also W24 and Hinrichs et al., 2017), and some NWES segments lack a minimum number of profiles to produce meaningful averages. For example, we are only able to estimate the on-shelf nitrate concentration in the PSBS segment in the spring (Figure 5a and Figure S2 in Supporting Information S1). The ocean-shelf nitrate gradient might also be sensitive to the choice of inshore isobath (100 m), but available cross-shelf resolving measurements (e.g., Ruiz-Castillo et al., 2019; Painter, 2024) suggest modest cross-shelf nitrate gradients between the 200 and 100 m isobaths.

Another limitation is that the data sets are not available on the same time periods. The ADT, WOA23/EN4, and NSBC data sets cover respectively the 1995–2022, 1975–2022, and 1960–2014 periods. However, considering the steadiness of the cross-isobath geostrophic velocity derived from the decadal altimetry and hydrography fields and the weak decadal nitrate variability in the deep ocean since 2000 (W24's Figure 5), we believe the impact of the different time periods on the geostrophic velocities and geostrophic nitrate transports is small.

It is also worth considering how resolving higher frequency/smaller scale processes might influence our results. At sub-seasonal timescales, we expect mesoscale eddies and coastal-trapped wave modes to project on the density and sea surface height fields, which could lead to important net nitrate transports if those changes covary with nitrate fluctuations. Eddies can induce cross-isobath nitrate transport by cross-isobath advection or isopycnal stirring (e.g., Stewart & Thompson, 2016). At seasonal to decadal timescales, smaller-scale motions (smaller than ≈40–50 km) can also influence along-isobath pressure gradients, especially topographically-steered along-isobath flows associated with unresolved shelf-edge features such as canyons.

5. Summary and Conclusions

We find evidence of persistent ocean-shelf geostrophic volume and nitrate transports in the North West European Shelf (NWES) from climatological fields and satellite altimetry. These transports are maintained by a large-scale steric sea surface structure associated with lighter water masses present at both ends of the NWES edge (Figure 1). Warmer Eastern North Atlantic Water occupies the southern and western segments of the NWES edge, and fresher Baltic outflow-influenced waters occupy its northeast end, along the southern rim of the Norwegian Trench (Figures 2f, 2k, and 2p). Despite strong changes in vertical stratification due to seasonal homogenization and re-stratification, lateral density gradients and sea surface slopes have weak variability (Figures 2f–2y, and 3a). The weakly-varying sea surface slopes and lateral density gradients result in seasonally-persistent surface cross-isobath geostrophic flow patterns, with weak vertical shear (Figures 3b and 4a–e).

Nitrate distributions show stronger seasonality, both along the shelf edge and on the shelf (Figures 4f–4j, 5a). As a result, seasonality in ocean-shelf nitrate gradients dominates cross-shelf nitrate transport convergence, and hence potential temporal changes in shelf nitrate concentrations. In the northern segments of the NWES, the ocean-shelf nitrate gradient reverses in the winter, thus reversing the local nitrate tendency on the shelf (Figures 5a–5c). The magnitude of the geostrophic transports is O(1–10 mmol/s) of nitrate per meter along-isobath distance, similar to that of winter nitrate recharge by wind-driven Ekman transport (Figures 5b–5d, Table 1, W24). Importantly, however, the geostrophic ocean-shelf transport is steady year-round, while the wind-driven nitrate recharge is a wintertime mechanism.

At decadal timescales, the surface cross-isobath velocity and the sea surface height structure show a persistence similar to that observed at seasonal timescales, with the shelf-edge sea surface rising uniformly at a rate close to that of the global mean sea level (Figure 6). The NWES edge hydrography does show important decadal changes

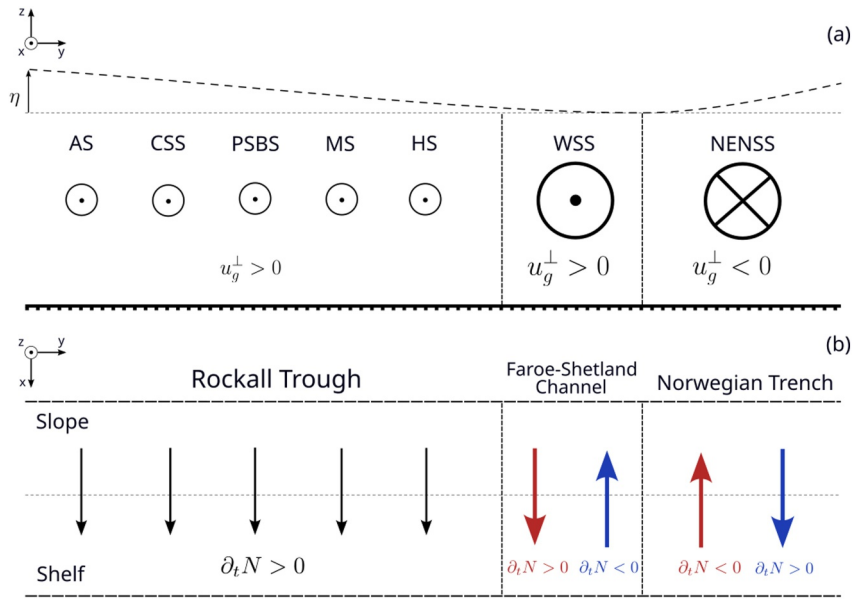

Figure 8. Schematic representation of the mechanisms involved in ocean-shelf geostrophic nitrate transport on the NWES. The ($\hat{x}$, $\hat{y}$, $\hat{z}$) directions are respectively cross-isobath (positive onshore), along-isobath (positive toward the Baltic Sea), and vertical (positive upward). (a) Along-isobath/vertical view (y, z). (b) Horizontal plan view (x, y). The large-scale slope in sea surface height η is indicated schematically, along with the sign of the depth-averaged cross-isobath geostrophic flow $\left(u_g^\perp\right)$ and of the nitrate tendency due to geostrophic cross-shelf nitrate transport convergence/divergence ($\partial_t N$). Red (blue) indicates the autumn/spring/summer (winter) nitrate tendency regime. AS = Armorican Shelf, CSS = Celtic Sea Shelf, PSBS = Porcupine Sea Bight Shelf, MS = Malin Shelf, HS = Hebrides Shelf, WSS = West Shetland Shelf, NENSS = North East North Sea Shelf.

related to the imprint of gyre-scale processes in the Subpolar North Atlantic, such as the recent subtropicalization of water masses in the Rockall Trough (e.g., Clark et al., 2022) and the large freshwater anomaly in the mid-2010s (e.g., Holliday et al., 2020). However, these steric imprints on the NWES edge result only in modest changes in steric height and cross-isobath geostrophic shear/transport, partly because the stratification changes have large along-isobath scales (Figure 7). This is consistent with the idea that the shape of the along-isobath sea surface height is set by time-mean density gradients modulated by shelf-wide, wind-driven modes of sea surface height variability transmitted by fast Kelvin and coastal-trapped waves (Diabaté et al., 2025; Hughes et al., 2019; Wise et al., 2024).

The picture that emerges is that of a perennial cross-shelf geostrophic circulation that represents a reliable source of new nitrate for the southern and western NWES, with wintertime reversals in the northern NWES associated with changes in ocean-shelf nitrate gradients. This low-frequency mechanism adds to our present understanding of ocean-shelf exchange on the NWES, where the contributions of several other processes have been estimated (e.g., Huthnance et al., 2022, and references therein, W24). Figure 8 summarizes our main findings schematically.

While shelf-wide estimates of exchange processes and their biogeochemical effects often require closed budgets derived from numerical models (e.g., Wakelin et al., 2012), mechanistic understanding of individual processes is essential for evaluating the realism of model estimates and for understanding their physical drivers. This understanding is thus necessary for predicting changes in circulation, primary production, atmospheric CO_2 drawdown, carbon burial, and carbon export to the deep ocean on the NWES and other continental shelves, with significant implications for the global carbon cycle (Legge et al., 2020; Roobaert et al., 2024). Geostrophic cross-isobath transport is likely an important component of these fluxes and their climate-scale variability on the NWES, and potentially elsewhere in the global coastal ocean.

Conflict of Interest

The authors declare no conflicts of interest relevant to this study.

Data Availability Statement

Code necessary to reproduce all results is available from https://github.com/apaloczy/xshelfGeostrophicTransportNWES, archived under https://doi.org/10.5281/zenodo.18199136. The World Ocean Atlas 2023 temperature, salinity, and nitrate data sets are available from the National Centers for Environmental Information/NOAA website, https://www.ncei.noaa.gov/access/world-ocean-atlas-2023/ (Garcia et al., 2024; Locarnini et al., 2024; Reagan et al., 2024). The North Sea Biogeochemical Climatology is available from the University of Hamburg website, https://www.cen.uni-hamburg.de/en/icdc/data/ocean/nsbc.html (Hinrichs et al., 2017). The EN4 temperature and salinity profile data set includes the bias correction from Gouretski and Reseghetti (2010) and is available from UKMO (2025). The regional ADT and MDT products for European seas are distributed by the Copernicus Marine Environment Monitoring Service (CMEMS, 2024a; CMEMS, 2024b). The SRTM15+ data set is available from the Institute of Geophysics and Planetary Physics (IGPP, 2025).

Acknowledgments
Palóczy and Hopkins were funded by the NERC National Capability Programme Atlantic Climate and Environment Strategic Science (AtlantiS), NE/Y005589/1. Thanks to ICDC, CEN, University of Hamburg for data support (NSBC climatology). This study has been conducted using E.U. Copernicus Marine Service Information; https://doi.org/10.48670/mds-00337, https://doi.org/10.48670/moi-00141. EN.4.2.2 data were obtained from https://www.metoffice.gov.uk/hadobs/en4/ and are © British Crown Copyright, Met Office, 2025, provided under a Non-Commercial Government License http://www.nationalarchives.gov.uk/doc/non-commercial-government-licence/version/2/. The authors thank the three anonymous reviewers for their input, which has helped improve the manuscript.

References

Ballarotta, M., Ubelmann, C., Pujol, M.-I., Taburet, G., Fournier, F., Legeais, J.-F., et al. (2019). On the resolutions of ocean altimetry maps. *Ocean Science*, *15*(4), 1091–1109. https://doi.org/10.5194/os-15-1091-2019

Brink, K. H. (2023). *Physical oceanography of Continental shelves* (1st ed.). Princeton University Press.

Calafat, F. M., Chambers, D. P., & Tsimplis, M. N. (2012). Mechanisms of decadal sea level variability in the eastern North Atlantic and the Mediterranean Sea. *Journal of Geophysical Research*, *117*(C9). https://doi.org/10.1029/2012JC008285

Clark, M., Marsh, R., & Harle, J. (2022). Weakening and warming of the European Slope Current since the late 1990s attributed to basin-scale density changes. *Ocean Science*, *18*(2), 549–564. https://doi.org/10.5194/os-18-549-2022

CMEMS. (2024a). European Seas gridded L4 Sea surface heights and derived variables reprocessed 1993 ongoing. *Marine Data Store [MDS]*. E. U. Copernicus Marine Service Information (CMEMS). https://doi.org/10.48670/moi-00141

CMEMS. (2024b). European Seas mean dynamic topography. (E.U. Copernicus Marine Service Information (CMEMS). *Marine Data Store [MDS]*. https://doi.org/10.48670/mds-00337

Connolly, T. P., Hickey, B. M., Shulman, I., & Thomson, R. E. (2014). Coastal trapped waves, alongshore pressure gradients, and the California undercurrent. *Journal of Physical Oceanography*, *44*(1), 319–342. https://doi.org/10.1175/JPO-D-13-095.1

Diabaté, S. T., Fraser, N. J., White, M., Berx, B., Marié, L., & McCarthy, G. D. (2025). On the wind-driven European shelf sea-level variability and the associated oceanic circulation, *291*, 105466. https://doi.org/10.1016/j.csr.2025.105466

Fraser, N. J., Cunningham, S. A., Drysdale, L. A., Inall, M. E., Johnson, C., Jones, S. C., et al. (2022). North Atlantic Current and European slope Current circulation in the rockall trough observed using moorings and gliders. *Journal of Geophysical Research: Oceans*, *127*(12), e2022JC019291. https://doi.org/10.1029/2022JC019291

Frederikse, T., Landerer, F. W., Caron, L., Adhikari, S., Parkes, D., Humphrey, V. W., et al. (2020). The causes of sea-level rise since 1900. *Nature*, *584*(7821), 393–397. https://doi.org/10.1038/s41586-020-2591-3

Garcia, H. E., Bouchard, C., Cross, S. L., Paver, C. R., Reagan, J. R., Boyer, T. P., et al. (2024). World ocean atlas 2023, volume 4: Dissolved inorganic nutrients (phosphate, nitrate, silicate). *National Centers for Environmental Information*, *92*. https://doi.org/10.25923/39qw-7j08

Good, S. A., Martin, M. J., & Rayner, N. A. (2013). EN4: Quality controlled ocean temperature and salinity profiles and monthly objective analyses with uncertainty estimates. *Journal of Geophysical Research: Oceans*, *118*(12), 6704–6716. https://doi.org/10.1002/2013JC009067

Gouretski, V., & Reseghetti, F. (2010). On depth and temperature biases in bathythermograph data: Development of a new correction scheme based on analysis of a global ocean database. *Deep-Sea Research*, *57*(6), 812–833. https://doi.org/10.1016/j.dsr.2010.03.011

Graham, J. A., Rosser, J. P., O'Dea, E., & Hewitt, H. T. (2018). Resolving Shelf break exchange around the European Northwest Shelf. *Geophysical Research Letters*, *45*(22), 12386–12395. https://doi.org/10.1029/2018GL079399

Hinrichs, I., Gouretski, V., Paetsch, J., Emeis, K., & Stammer, D. (2017). North Sea Biogeochemical Climatology (Version 1.1). Retrieved from https://doi.org/10.1594/WDCC/NSBClim_v1.1

Holliday, N. P., Bersch, M., Berx, B., Chafik, L., Cunningham, S., Florindo-López, C., et al. (2020). Ocean circulation causes the largest freshening event for 120 years in eastern subpolar North Atlantic. *Nature Communications*, *11*(1), 585. https://doi.org/10.1038/s41467-020-14474-y

Holt, J., Harle, J., Wakelin, S., Jardine, J., & Hopkins, J. (2022). Why is seasonal density stratification in Shelf Seas expected to increase under future climate change? *Geophysical Research Letters*, *49*(23), e2022GL100448. https://doi.org/10.1029/2022GL100448

Holt, J., Polton, J., Huthnance, J., Wakelin, S., O'Dea, E., Harle, J., et al. (2018). Climate-Driven change in the North Atlantic and Arctic Oceans can greatly reduce the circulation of the North Sea. *Geophysical Research Letters*, *45*(21), 11827–11836. https://doi.org/10.1029/2018GL078878

Holt, J., & Proctor, R. (2008). The seasonal circulation and volume transport on the northwest European continental shelf: A fine-resolution model study. *Journal of Geophysical Research*, *113*(C6). https://doi.org/10.1029/2006JC004034

Hughes, C. W., Fukumori, I., Griffies, S. M., Huthnance, J. M., Minobe, S., Spence, P., et al. (2019). Sea level and the role of coastal trapped waves in mediating the influence of the open ocean on the coast. *Surveys in Geophysics*, *40*(6), 1467–1492. https://doi.org/10.1007/s10712-019-09535-x

Huthnance, J., Hopkins, J., Berx, B., Dale, A., Holt, J., Hosegood, P., et al. (2022). Ocean shelf exchange, NW European shelf seas: Measurements, estimates and comparisons. *Progress in Oceanography*, *202*, 102760. https://doi.org/10.1016/j.pocean.2022.102760

IGPP (2025). Global bathymetry and topography at 15 Arc Sec. In *(SatelliteGeodesyResearchGroupatthe Cecil H. and. Ida, M. Institute of Geophysics and Planetary Physics (IGPP), Scripps institution of oceanography, university of California San Diego (SIO/UCSD)*. Dataset version SRTM15+V2.7 Retrieved in May/2025). https://topex.ucsd.edu/pub/srtm15_plus/SRTM15_V2.7.nc

Johnson, C., Fraser, N., Cunningham, S., Burmeister, K., Jones, S., Drysdale, L., et al. (2024). Biogeochemical properties and transports in the North East Atlantic. *Journal of Geophysical Research: Oceans*, *129*(4), e2023JC020427. https://doi.org/10.1029/2023JC020427

Jones, S. C., Cottier, F., Inall, M. E., & Griffiths, C. (2018). Decadal variability on the Northwest European continental shelf. *Progress in Oceanography*, *161*, 131–151. https://doi.org/10.1016/j.pocean.2018.01.012

Jones, S. C., Fraser, N. J., Cunningham, S. A., Fox, A. D., & Inall, M. E. (2023). Observation-based estimates of volume, heat, and freshwater exchanges between the subpolar North Atlantic interior, its boundary currents, and the atmosphere. *Ocean Science*, *19*(1), 169–192. https://doi.org/10.5194/os-19-169-2023

Kelly, S., Popova, E., Yool, A., Jebri, F., Oliver, S., & Srokosz, M. (2025). Abrupt changes in the timing and magnitude of the north Atlantic bloom over the 21st century. *Journal of Geophysical Research: Oceans*, *130*(3), e2024JC022284. https://doi.org/10.1029/2024JC022284

LaCasce, J. H., & Groeskamp, S. (2020). Baroclinic modes over rough bathymetry and the surface deformation radius. *Journal of Physical Oceanography*, *50*(10), 2835–2847. https://doi.org/10.1175/JPO-D-20-0055.1

Legge, O., Johnson, M., Hicks, N., Jickells, T., Diesing, M., Aldridge, J., et al. (2020). Carbon on the Northwest european Shelf: Contemporary budget and future influences. *Frontiers in Marine Science*, *7*, 7–2020. https://doi.org/10.3389/fmars.2020.00143

Levitus, S., Antonov, J. I., Boyer, T. P., Baranova, O. K., Garcia, H. E., Locarnini, R. A., et al. (2012). World ocean heat content and thermosteric sea level change (0–2000 m), 1955–2010. *Geophysical Research Letters*, *39*(10). https://doi.org/10.1029/2012GL051106

Liao, F., Liang, X., Li, Y., & Spall, M. (2022). Hidden upwelling systems associated with major Western boundary currents. *Journal of Geophysical Research: Oceans*, *127*(3), e2021JC017649. https://doi.org/10.1029/2021JC017649

Liu, K.-K., Atkinson, L., Quiñones, R. A., & Talaue-McManus, L. (2010). Biogeochemistry of continental margins in a global context. In K.-K. Liu, L. Atkinson, R. Quiñones, & L. Talaue-McManus (Eds.), *Carbon and nutrient fluxes in continental margins: A global synthesis* (pp. 3–24). Springer Berlin Heidelberg. https://doi.org/10.1007/978-3-540-92735-8_1

Locarnini, R. A., Mishonov, A. V., Baranova, O. K., Reagan, J. R., Boyer, T. P., Seidov, D., et al. (2024). World ocean atlas 2023, volume 1: Temperature. *National Centers for Environmental Information*, *89*. https://doi.org/10.25923/54bh-1613

Marsh, R., Haigh, I. D., Cunningham, S. A., Inall, M. E., Porter, M., & Moat, B. I. (2017). Large-scale forcing of the European Slope Current and associated inflows to the North Sea. *Ocean Science*, *13*(2), 315–335. https://doi.org/10.5194/os-13-315-2017

Moncuquet, A., Jones, N. L., Bordois, L., Dufois, F., & Lazure, P. (2025). Observations of cross-shelf transport due to internal wave pumping on the Bay of Biscay shelf. *Ocean Science*, *21*(6), 3375–3395. https://doi.org/10.5194/os-21-3375-2025

Nerem, R. S., Beckley, B. D., Fasullo, J. T., Hamlington, B. D., Masters, D., & Mitchum, G. T. (2018). Climate-change–driven accelerated sea-level rise detected in the altimeter era. *Proceedings of the National Academy of Sciences*, *115*(9), 2022–2025. https://doi.org/10.1073/pnas.1717312115

Painter, S. C. (2024). Observations of phytoplankton productivity and growth rates in the Malin shelf break environment. *Continental Shelf Research*, *279*, 105281. https://doi.org/10.1016/j.csr.2024.105281

Pauly, D., Christensen, V., Guénette, S., Pitcher, T. J., Sumaila, U. R., Walters, C. J., et al. (2002). Towards sustainability in world fisheries. *Nature*, *418*(6898), 689–695. https://doi.org/10.1038/nature01017

Piecuch, C. G., Fukumori, I., Ponte, R. M., Schindelegger, M., Wang, O., & Zhao, M. (2022). Low-Frequency dynamic Ocean response to barometric-pressure loading. *Journal of Physical Oceanography*, *52*(11), 2627–2641. https://doi.org/10.1175/JPO-D-22-0090.1

Porter, M., Dale, A. C., Jones, S., Siemering, B., & Inall, M. E. (2018). Cross-slope flow in the Atlantic Inflow Current driven by the on-shelf deflection of a slope current. *Deep-Sea Research*, *140*, 173–185. https://doi.org/10.1016/j.dsr.2018.09.002

Pujol, M.-I., Faugère, Y., Taburet, G., Dupuy, S., Pelloquin, C., Ablain, M., & Picot, N. (2016). Duacs DT2014: The new multi-mission altimeter data set reprocessed over 20 years. *Ocean Science*, *12*(5), 1067–1090. https://doi.org/10.5194/os-12-1067-2016

Reagan, J. R., Seidov, D., Wang, Z., Dukhovskoy, D., Boyer, T. P., Locarnini, R. A., et al. (2024). World ocean atlas 2023, volume 2: Salinity. *National Centers for Environmental Information*, *90*. https://doi.org/10.25923/70qt-9574

Roobaert, A., Resplandy, L., Laruelle, G. G., Liao, E., & Regnier, P. (2024). Unraveling the physical and biological controls of the global coastal CO2 sink. *Global Biogeochemical Cycles*, *38*(3), e2023GB007799. https://doi.org/10.1029/2023GB007799

Ruiz-Castillo, E., Sharples, J., Hopkins, J., & Woodward, M. (2019). Seasonality in the cross-shelf physical structure of a temperate shelf sea and the implications for nitrate supply. *Progress in Oceanography*, *177*, 101985. https://doi.org/10.1016/j.pocean.2018.07.006

Simpson, J., & Bowers, D. (1981). Models of stratification and frontal movement in shelf seas. *Deep-Sea Research*, *28*(7), 727–738. https://doi.org/10.1016/0198-0149(81)90132-1

Simpson, J., & Sharples, J. (2012). *Introduction to the physical and biological oceanography of Shelf Seas*. Cambridge University Press. https://doi.org/10.1017/CBO9781139034098

Song, Y., Lin, Y., Zhan, P., Liu, Z., & Cai, Z. (2025). Interannual variability of summertime cross-isobath exchanges in the northern South China Sea: ENSO and riverine influences. *Ocean Science*, *21*(6), 3361–3374. https://doi.org/10.5194/os-21-3361-2025

Spingys, C. P., Williams, R. G., Hopkins, J. E., Hall, R. A., Green, J. A. M., & Sharples, J. (2020). Internal tide-driven tracer transport across the Continental slope. *Journal of Geophysical Research: Oceans*, *125*(9), e2019JC015530. https://doi.org/10.1029/2019JC015530

Stewart, A. L., & Thompson, A. F. (2016). Eddy generation and jet Formation via dense water outflows across the antarctic Continental slope. *Journal of Physical Oceanography*, *46*(12), 3729–3750. https://doi.org/10.1175/JPO-D-16-0145.1

Stock, C. A., John, J. G., Rykaczewski, R. R., Asch, R. G., Cheung, W. W. L., Dunne, J. P., et al. (2017). Reconciling fisheries catch and ocean productivity. *Proceedings of the National Academy of Sciences*, *114*(8), E1441–E1449. https://doi.org/10.1073/pnas.1610238114

Tozer, B., Sandwell, D. T., Smith, W. H. F., Olson, C., Beale, J. R., & Wessel, P. (2019). Global bathymetry and topography at 15 arc sec: SRTM15+. *Earth and Space Science*, *6*(10), 1847–1864. https://doi.org/10.1029/2019EA000658

UKMO. (2025). *EN4: Quality controlled subsurface ocean temperature and salinity profiles and objective analyses*. Met Office Hadley Centre. Retrieved from https://www.metoffice.gov.uk/hadobs/en4(versionEN.4.2.2

Wakelin, S. L., Holt, J. T., Blackford, J. C., Allen, J. I., Butenschön, M., & Artioli, Y. (2012). Modeling the carbon fluxes of the northwest European continental shelf: Validation and budgets. *Journal of Geophysical Research*, *117*(C5). https://doi.org/10.1029/2011JC007402

Wang, J., Fu, L.-L., Qiu, B., Menemenlis, D., Farrar, J. T., Chao, Y., et al. (2018). An observing system simulation experiment for the calibration and validation of the surface water ocean topography sea surface height measurement using in situ platforms. *JAOT*, *35*(2), 281–297. https://doi.org/10.1175/JTECH-D-17-0076.1

Wei, X., Hopkins, J., Oltmanns, M., Johnson, C., & Inall, M. (2024). The role of deep Winter mixing and wind-driven surface Ekman Transport in supplying Oceanic nitrate to a temperate Shelf Sea. *Journal of Geophysical Research: Oceans*, *129*(1), e2022JC019518. https://doi.org/10.1029/2022JC019518

Wise, A., Calafat, F. M., Hughes, C. W., Jevrejeva, S., Katsman, C. A., Oelsmann, J., et al. (2024). Using shelf-edge transport composition and sensitivity experiments to understand processes driving Sea level on the Northwest European Shelf. *Journal of Geophysical Research: Oceans*, *129*(5), e2023JC020587. https://doi.org/10.1029/2023JC020587